RSC Advances

ROYAL SOCIETY OF CHEMISTRY

www.rsc.org/advances

RSC Advances

PAPER

Oxygen vacancies modified TiO_2 nanoparticles as enhanced visible-light driven photocatalyst by wrapping and chemically bonding with graphite-like carbon

2jiushiReceived 00th January 2015,
Accepted 00th January 2015

DOI: 10.1039/x0xx00000x

www.rsc.org/advances

Xiuqi Qin[a], Fang He*[a], Lixia Chen[a], Yuhuan Meng[a], Jing Liu[a], Naiqin Zhao[a], Yuan Huang[a]

To gain commendable photocatalyst from inexpensive materials has always been the goal that researchers are struggling for. In this paper, an effective visible-light driven composite photocatalyst (TC800) composed of TiO_2 nanocrystallines and graphite-like carbon was prepared using titanium tetrachloride and glucose as raw materials via hydrothermal method and subsequent annealing at 800 ^oC. The results show the TiO_2 nanocrystallines in the prepared photocatalyst are wrapped and chemically bonded with graphite-like carbon. More importantly, oxygen vacancies are successfully introduced into TiO_2 nanocrystallines. The two aspects as well as the enhanced graphitization of carbon make TC800 possess better photocatalytic activity compared to the as-prepared sample without annealing, by degradating rhodamine b (RhB) under visible light. What's more, when taking the mass of the dye and the corresponding photocatalyst into consideration, the nanocomposites present 4 times higher photocatalytic activity than the previously reported TiO_2/non-graphene carbon compounds. Thus, the nanocomposites proposed in this paper will be a good alternative in the field of visible-light driven photocatalysis, and this work also provides further insights into the modification of TiO_2.

Introduction

Titania (TiO_2) / carbon composites (TCC) have been one of the research focuses for a long time, especially in the field of visible-light photocatalysis, due to the special properties of both TiO_2 and carbon. As reported, TiO_2 possesses commendable performance in terms of chemical inertness, strong oxidizing activity, long-term stability against photocorrosion, cost effectiveness and nontoxicity,[1,2] which contributes to its wide application in photocatalysis[3]. While its application is greatly limited due to the poor visible light response and high charge recombination rate, resulting from its wide band gap (3.2 eV for anatase and 3.0 eV for rutile) and the relatively low electrical conductivity. It has been reported that when TiO_2 is combined with carbon species such as graphene, reduced graphene oxide and graphite-like carbon to form TCC, its visible light absorption and charge transmission ability can be exactly improved to some extent,[4-6] because carbon materials generally present relatively high light absorption ability, abundant active sites,[7,8] and the fast mobility of charge carriers. Further studies have indicated that photocatalytic performance of TCC can also be affected by the chemical binding formed between TiO_2 and carbon materials.[9,10] It has been proven that the chemical binding at the interface is effective to decrease the potential barrier that required to overcome when charge carriers transfer within TiO_2 material, contributing to the rapid transmission of photo-generated electron-hole pairs.[10] Huang et al. found that the photocatalytic performance of TiO_2/graphene composites could be increased by 1.5 times when TiO_2 was chemically bonded with graphene, which was attributed to interfacial charge transfer through chemical bond.[10] At the same time, carbon materials with good conductivity can not only act as electron acceptor[11] but also provide the "high-way" for carriers' transport, which reduce the recombination of charge carriers, leading to enhanced photocatalytic performance of TCC. Thus it is easily believed that carbon materials with good conductivity will further improve photocatalytic performance of TCC.

In addition to the above two aspects, it has also found that crystal defects in pure TiO_2 are closely related to its photocatalytic performance.[12,13] Among the defects, oxygen vacancies which usually accompany with Ti^{3+} are supposed to be one of the most important defects. On one hand, oxygen vacancies are verified beneficial to the light absorption[14] and the separation of carriers,[11] facilitating the redox reaction. On the other hand, they can introduce intermediate level and contribute to a narrow band gap of the semiconductor,[15,16] thus leading to low charge recombination rate and high quantum efficiency. Therefore, different strategies are conducted to induce oxygen vacancies, such as

[a] Tianjin Key Laboratory of Composite and Functional Materials, Department of Materials Science and Engineering, Tianjin University, Tianjin, 300072, P. R. China. Email: fanghe_tju@tju.edu.cn

Electronic Supplementary Information (ESI) available: [details of any supplementary information available should be included here]. See DOI: 10.1039/x0xx00000x

hydrogenation,[17] high energy particle bombardment,[18] annealing[19,20] etc. In particular, annealing under oxygen depleted condition has attracted much attention because the concentration of oxygen vacancies goes up with the decrease of O_2 pressure, according to the standard Kr¨oger–Vink notation.[21] Thus, as to TCC, it is firmly believed that the photocatalytic property under visible light irradiation will be further enhanced if oxygen vacancies can be successfully introduced to TiO_2 nanoparticles.

Here, we synthesized TiO_2/carbon nanocomposites using cheap raw materials including glucose, titanium tetrachloride , ethanol and water via a facile solvothermal method followed by annealing at 800 ^oC. TiO_2 nanocrystallines are not only wrapped by graphite-like carbon, but also chemically bonded with it through Ti-O-C. More importantly, oxygen vacancies in TiO_2 are observed in the nanocomposites. Meanwhile, it is proposed that the enhancement of the photocatalytic activity is mainly the results of the combined effects of the graphite-like carbon, chemical binding between TiO_2 and carbon materials, and the oxygen vacancies in TiO_2 by designing control sample.

Experimental

Chemicals

Titanium tetrachloride (AR), anhydrous glucose (AR) and absolute ethanol (AR) were purchased from Tianjin Guangfu Technology Development Co. LTD. All chemicals were used without further purification.

Preparation of samples

Hydrothermal process combined with annealing was employed to obtain the efficient catalyst. All regents were used without any further purification. Given the fact that the annealing temperature had deep effect on the performance of catalysts,[6,16] a series of experiments with the single variable of different glucose concentrations or temperatures were conducted to figure out the most appropriate one (Fig. S1). In a typical synthesis, 2.2 mL of $TiCl_4$ was injected into 7.8 mL of ethanol under vigorous stirring to make clear solution (solution 1). Meanwhile, 5.4 g glucose was dissolved into 60 mL water assisted by magnetic stirring as well until solution 2 was achieved. Later we added solution 1 to solution 2 dropwise and kept it stirring for 1 h. Then the mixed solution was subsequently transferred to a 100 mL autoclave and hydrothermally treated at 190 ^oC for 4 h. After cooling along with the furnace to an ambient temperature, the brownish black precipitation was collected and washed with deionized water and ethanol three times respectively and dried at 80 ^oC in an oven overnight. Afterwards the precipitation was heated at 800 ^oC for 2 h under Ar flow and finally the product (named as TC800) was synthesized. For comparison, the control sample (named as TC), which was prepared in the absence of annealing while other conditions were the same as TC800, was investigated as well.

Photoelectrodes preparation

In brief, 2 mL ethanol and 0.2 mL Nafion were mixed under stirring for 30 min. Then 15 mg of photocatalyst was suspended in the solution with the aid of ultraphonic until a slurry was achieved. Afterwards, the slurry was dip-coated onto a 1 cm×2 cm indium-tin oxide (ITO) glass electrode, and the electrode was placed at room temperature for 2 h to vaporize ethanol. Pt foil, Ag/AgCl electrode and photocatalysts were placed in the reactor as counter, reference and working electrodes respectively. Prior to the measurements, the electrolyte (0.5M Na_2SO_4) was poured into the reactor.

Characteristics

X-ray diffraction (XRD) patterns were performed on a Rigaku D/max diffractometer with Cu Kα radiation (λ = 0.15418 nm) at a scan rate of 6 ^oC/min and the range of 2θ angles was from 10 ^oC to 90 ^oC. The accelerating voltage and the applied current were 40 KV and 40 mA, respectively. Transmission electron microscopy (TEM) observation taken on a FEI Tecnai G2 F20 TEM operating at 200 KV accelerating voltage was conducted to investigate the morphology of products. TGA was performed with a Perkin-Elmer (TA Instruments) instrument up to 800 ^oC at a heating rate of 10 ^oC /min in air to detect the actual mass ratio of carbon in the composites. The Raman spectrum was recorded on the LabRAM HR Raman spectrometer with exciting wavelength at 532 nm. Energy-dispersive X-ray spectroscopy (EDX) analyses of the composites were carried out with spatially resolved EDX spectrum attached to a TDCLS-4800 SEM (Hitachi). X-ray photoelectron spectroscopy (XPS; PHI 5000Versa-Probe) analysis was conducted using monochromatized AlKα radiation (1486.6 eV). Nitrogen adsorption–desorption isotherms and BET surface area were measured at 77 K with an ASAP 2020 physisorption analyser (USA). UV-vis diffuse reflectance spectra were obtained using a scan UV-vis spectrophotometer (UV-2700, Shimadzu) equipped with an integrating sphere assembly.

Photocatalytic activity

The photocatalytic activities were conducted at room temperature under the visible light (λ > 400 nm) from a 350 W Xe lamp equipped with a cutoff filter. Briefly, 5 mg of the photocatalyst was dispersed in 40 mL of a 10 mg/L aqueous solution of RhB in a reactor cooled by running water to keep the temperature unchanged. Before illumination, the suspension was magnetically stirred in the dark for 30 min to make sure the establishment of an adsorption/desorption equilibrium between the photocatalyst and RhB. Then the suspension was exposed to the Xe lamp along with magnetic

stirring. At given time intervals, about 0.5 ml aliquots were sampled, centrifuged and monitored with the UV-2700 spectrophotometer (Shimadzu). The degradation rate *D* of RhB was calculated as follows:

$$D = (C_o\text{-}C) / C_o * 100\% \quad (1)$$

where *C* was the concentration of RhB at the irradiation time *t* and C_o represented the concentration in the adsorption equilibrium of the photocatalyst before irradiation. To further evaluate the photocatalytic efficiency, the mass of the dye as well as the corresponding catalyst was taken into account, and a new parameter D_1 was introduced and defined as follows:

$$D_1 = D / (m * m^{-1}_{dye} * t) \quad (2)$$

where *m* was the mass of the catalyst used, m_{dye} was the mass of the dye and *t* was the irradiation time. To study the stability of the catalyst, repeat experiments on RhB degradation were performed. After each cycle, the catalyst was separated from the solution by centrifugation and washed with water and ethanol. Then they were redispersed in a fresh dye solution for another cycle.

Results and discussion

Enhanced photocatalytic performance

The enhanced photocatalytic performance of TC800 was evaluated by degrading RhB under visible-light irradiation. In addition, experiments to ascertain the self-degradation of RhB and the requirement of illumination were conducted at the meantime. From Fig. 1(a), it can be seen that no obvious degradation of RhB is detected when the suspension is stirred in dark or irradiated under visible light in the absence of TC800. While, when in the presence of TC800, the degradation rate of RhB is calculated to be 64.5% after irradiation for 150 min (the UV-vis absorption spectrums of TC800 at given time intervals are illustrated in Fig. 1(b)). These results indicate that it is TC800 that utilizes visible light to degrade RhB. As a control, the catalytic performances of Degussa P25 TiO_2 (surface area of 52.53 m^2/g)[22] and TC (surface area of 222 m^2/g, Fig.1(c)) were assessed as well. As shown, TC800 exhibits the highest visible light photocatalytic activity, according to Equation (1). In addition, the degradation efficiency of RhB by different photocatalysts are also characterized (Table S1) using Equitation (2) by taking the mass of the dye and the catalyst used into consideration. And the larger value of D_1 is, the higher efficiency approaches. As the results suggest, the as-prepared TC800 significantly outperforms the previously reported TiO_2/non-graphene carbon compounds[23,24] by a factor of 4. To find out the reason for the better performance of TC800 than that of TC in visible light degradation, detailed characterizations were carried out. The stability and repeatability of TC800 were later examined by performing the recycling experiments. As shown in Fig. 1(d), no obvious decrease in the degradation rate is observed after five cycles, indicating the catalyst exhibits good stability after a long time irradiation.

Structure and Morphology of TC800

The crystal structure and composition of TC800 were identified by XRD, and the result of TC was included for comparison. As shown in Fig. 2, similar to TC, all the peaks of TC800 are indexed to anatase TiO_2 (JCPDS: 21-1272). It is known that the phase transition of TiO_2 from anatase to rutile occurs at around 600 °C. While, in this study, TiO_2 nanoparticles in TC800 still maintain the anatase phase after annealed at 800 °C, which can be ascribed to the carbon outside of TiO_2 nanoparticles, suppressing the phase transition of TiO_2 at high temperatures.[25,26] Compared to the pattern of TC, TC800 shows higher and narrower peaks, suggesting a better crystallinity of TiO_2 is obtained. Through Scherer equation calculation, although the average crystal size of TiO_2 changes from 6.3 nm to 9.0 nm after annealing, it is still much smaller than that of TiO_2 crystals in TCC studied by Shanmugam et al..[25]

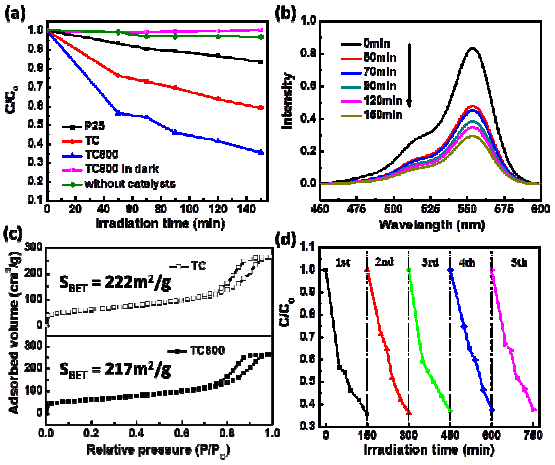

Fig. 1 (a) Photocatalytic degradation of RhB over different photocatalysts under the irradiation of visible light, (b) the time-dependent absorption spectra of RhB in the presence of TC800 (c) Nitrogen adsorption–desorption isotherms of TC and TC800 (d) Five-cycle photocatalytic degradation of RhB over TC800

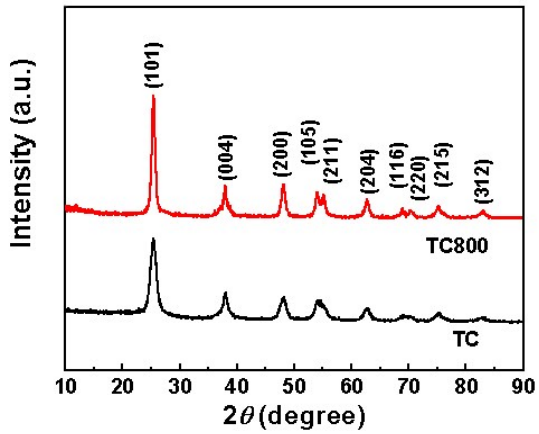

Fig. 2 XRD patterns of TC and TC800 nanocomposites.

Thus it can be proposed that carbon layers outside of TiO_2 show obvious inhibition on crystal growth of TiO_2.

The morphologies of TC800 and TC were examined with high-resolution transmission electron microscopy (HRTEM) to explore the influence of annealing. In Fig. 3(a), it is easily found that TiO_2 crystals with the interplanar spacing of 0.349 nm (which matches well with the (101) planes of anatase TiO_2) are wrapped by the amorphous carbon layers. While the carbon layer in TC800 displays a wavy morphology, which is a typical characteristic of graphite-like carbon. According to the previous study,[6] graphite-like carbon contributes to the enhancement of catalytic activity. Thus, it is firmly believed that the partly graphitized carbon in TC800 resulting from the annealing process will help in the same way. Moreover, the HRTEM pictures also show that the crystal size of TiO_2 becomes larger after annealed at 800 ^{o}C, but it is still smaller than 10 nm, which is consistent with the XRD analysis above.

The nature of the carbon present in TC800 and TC was further studied by Raman spectroscopy and shown in Fig. 4. Both of the recorded spectra show two obvious Raman bands at 1598 cm^{-1} and 1345 cm^{-1}, which are important for presenting the nature of carbon materials. The band located at 1598 cm^{-1} corresponds to the *E2g* mode (stretching vibrations) in the basal plane of the crystalline graphite (*G* band).[27] While the one located at 1345 cm^{-1} (*D* band) is associated with the disorder within the graphitic structure. Moreover, the intensity ratio between D band and G band (I_D/I_G) is often utilized as an index to judge the degree of crystallinity of various carbon materials. And the smaller ratio of I_D/I_G is, the higher order in the carbon material approaches. Here, the I_D/I_G ratios for TC and TC800 are 0.91 and 0.85, respectively, demonstrating the improved crystallinity of carbon materials in TC800. The anatase TiO_2 vibrational spectrum with six Raman-active fundamentals are $E_{g\,(1)}$, $E_{g\,(2)}$, $E_{g\,(3)}$ at 144, 197, and 639 cm^{-1}, $B1_{g\,(1)}$, $B1_{g\,(2)}$ at 399 and 519 cm^{-1}, and $A1_{g\,(1)}$ mode at 513 cm^{-1}, respectively.[28] In Fig. 4, the peaks at 146, 399, 514 and 638 cm^{-1} are all indexed to pure TiO_2. However, in the Raman spectrum of TC800, the peak that should be located at 144 cm^{-1} for TiO_2 is found red shifted to 157 cm^{-1}, which is caused by a change in chemical environment of TiO_2, suggesting the existence of oxygen vacancies.[28]

To investigate the chemical environments of the photocatalysts in detail, XPS analysis of TC and TC800 was conducted and shown in Fig. 5. As for the C 1s spectra, the binding energy of 284.6 eV corresponding to C-C is found in both Fig. 5(a) and (d). The deconvoluted peaks in Fig. 5(a) centred at the binding energy of 285.9 and 289.0 eV areattributed to the surface C-OH[29] and C=O (COO).[30] While in Fig. 5(d), totally different peaks are deconvoluted. The binding centred at 285.5 eV is indexed to C-O,[31] indicating the incomplete carbonization. Another peak at 288.7 eV belongs to Ti-O-C bond,[10] which reveals the intimate interactionbetween TiO_2 and carbon layer due to the annealing process. As shown, there is no peak at around 282 eV in Fig. 5(d), implying the absence of Ti-C bond.[33,34] Fig. 5(b) and (e) display the Ti 2p XPS spectra of the composites before and after annealing. Different from the two peaks located at 458.5 eV and 464.3 eV in Fig. 5(b), which correspond to Ti 2p3/2 and Ti 2p1/2 respectively in pure TiO_2,[32] the counterparts in Fig. 5(e) exhibit a chemical shift of +0.9 eV. Since there is no peak related to Ti-C bond in neither C 1s nor Ti 2p spectra, the possibility of carbon atoms directly combined with titanium atom (in TiO_2) is roughly excluded. Therefore, carbon atoms may not interact with titanium atoms but the lattice oxygen in TiO_2. This is because the electronegativity of C is greater than that of Ti. Due to the decrease of the electron density around Ti atom resulted from the greater electronegativity of C via O working on Ti, the shielding effect is weakened, as a result, the binding energy increases.[35] The identical viewpoint is verified by the similar results of O 1s too. The binding energy of lattice oxygen in TC800 (Fig. 5(f)) is 530.7 eV, which is 1.0 eV higher than that of pure TiO_2 (529.7 eV),[36] displaying the same chemical shift. In addition, there are two extra peaks existing in O 1s spectra of TC800 (Fig. 5(f)). One at 532.4 eV shows the formation of oxygen vacancies,[37-39] which is in accord with the Raman analysis. However, no peaks related to Ti^{3+} are detected, which probably because Ti^{3+} is easily oxidized. The other peak at 288.7 eV corresponded to Ti-O-C[35] is in line with

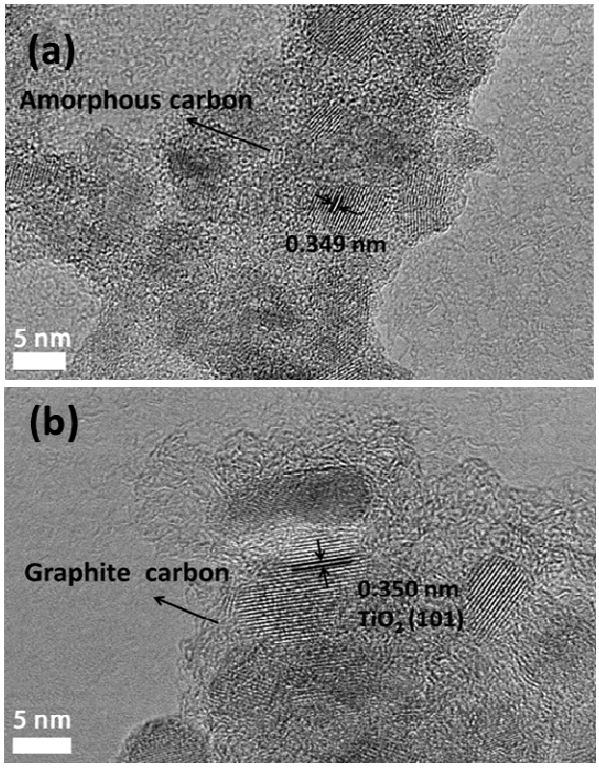

Fig. 3 HRTEM images of (a) TC and (b) TC800.

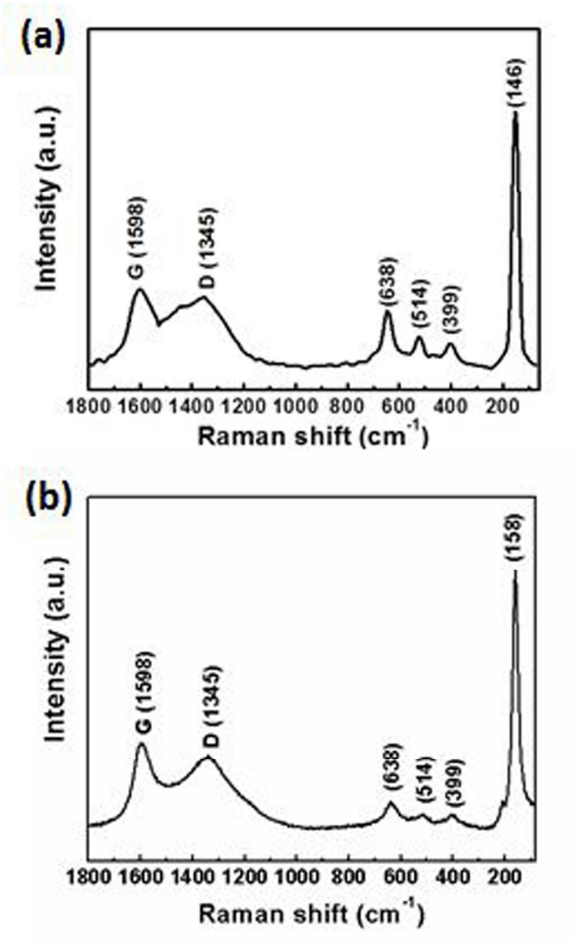

Fig. 4 (a) Raman spectrum of TC, (b) Raman spectrum of TC800 (inset shows an expanded part of the spectra which ranges from 200–800cm^{-1})

the above analysis. All the results suggest that the subsequent annealing has a significant impact on TC, contributing to the formation of oxygen vacancies in TiO_2 and chemical binding between TiO_2 and carbon layers.

Fig. 6 shows the TG-DSC curve of TC800 (with 18.3% carbon loading) and TC (32.1% carbon loaded), which were performed in air with a heating rate of 10 ^{o}C/min. With increasing temperature, TC shows a gradual mass loss until 420 ^{o}C and a very sharp exothermic peak at 397 ^{o}C in the DSC curve accompanies, suggesting the combustion of carbon layers. In contrast, TC800 exhibits a later onset of weight loss (~505 ^{o}C) than TC and an obvious exothermic peak centred at 450 ^{o}C (Fig. 6(b)). It is supposed that the chemical state changes verified by Raman and XPS analysis may contribute to the thermal stability of carbon. And probably the enhancement of thermal stability of the nanocomposite is resulted from the strong chemical coupling between carbon layer and TiO_2 nanocrystallines.[10] In addition, there is still an additional exothermic peak at 529.5 ^{o}C (as shown in Fig. 6(b)), which may results from the breakage of Ti-O-C bond. Likewise, the result

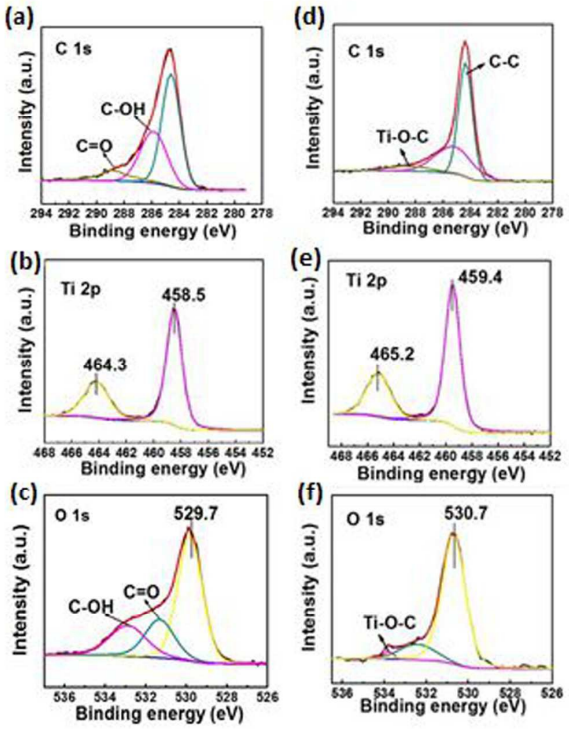

Fig. 5 X-ray photoelectron spectroscopy results of TC (a) C 1s, (b) Ti 2p, (c) O 1s spectra, and TC800 (d) C 1s, (e) Ti 2p, (f) O 1s spectra

is another persuasive evidence of the existence of Ti-O-C bond in TC800.

Consequently, it can be concluded that the graphite-like carbon, oxygen vacancies as well as the chemical binding between TiO_2 nanocrystallines and carbon layer have been simultaneously brought into TC800 by annealing, which probably lead to the enhanced visible light photocatalytic activity. And the proposal can be experimentally supported by UV-vis diffuse absorption spectra and the photocurrent test.

The responses of different catalysts to visible light were evaluated by UV–vis diffuse reflectance spectrograph. In Fig. 7(a), P25 displays an absorption edge around 400 nm as expected, and barely absorbs visible light. On the contrast, both TC and TC800 show improved visible-light absorption. When the wavelength starts from 900 nm, the absorption spectrum of TC shows a slow upward trend and reaches its summit when the wavelength is around 300 nm. The spectrum also shows a red shift in the absorpion edge of TC, which is attributed to the surface carbon layer modifying the TiO_2 nanocrystals.[39] While TC800 displays a continuous strong absorption in its whole spectrum(200-800 nm), indicating its excellent visible light absorption, which is attributed to the chemical binding,[40,41] oxygen vacancies[42] and graphite-like carbon.[6]

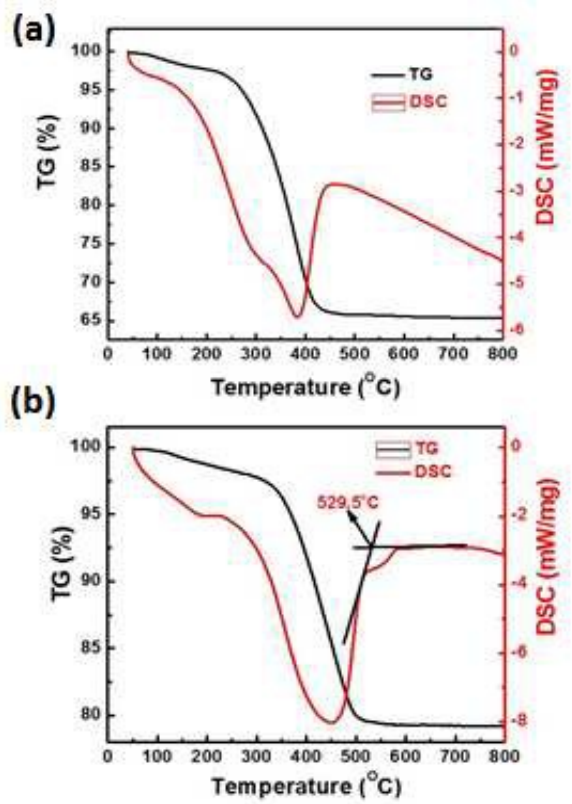

Fig. 6 The TG-DSC curves of TC (a) and TC800 (b)

Photocurrent measurements resulting from the separation of photoinduced charge transportation under the bias are powerful demonstrations of recombination efficiency. The tests were carried out for P25, TC and TC800 after deposition on ITO. The potential of the working electrode against a Pt counter electrode was set at 0.5 V. As the curves show, when light is on, the photocurrent density of all samples is significantly increased and stays through out the whole illumination. After the light is off, the photocurrent decreaces sharply due to the recombination of photo-induced carriers. Thus, the larger the curent is, the lower efficiency of recombination is. As shown in Fig. 8, both TC and TC800 show much higher current intensity than P25 under visible light irradiation. And the current intensity of TC800 is 1.9 times higher than that of TC, indicating the effective separation of the photo-generated electron–hole pairs under visible light, which can be attributed to the graphite-like carbon, chemical binding between TiO_2 and carbon, and oxygen vacancies in TiO_2.

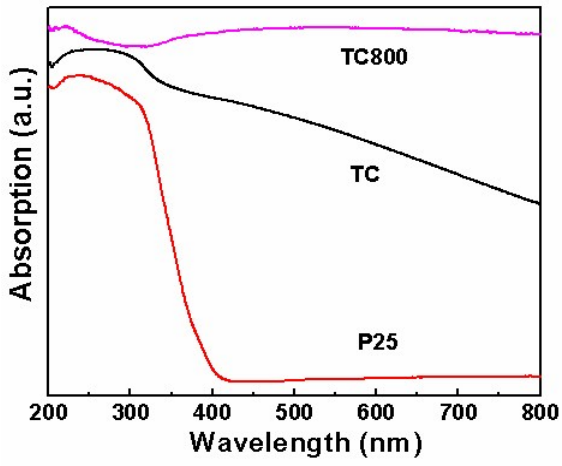

Fig. 7 The UV–Vis absorption spectra of TC800, TC and P25

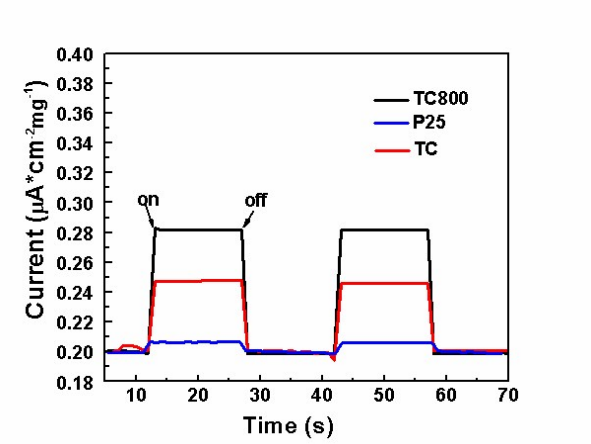

Fig. 8 Photoelectrochemical responses of TC800, TC and P25 electrodes under visible light irradiation. Input power = 100 mW/ cm^2, the bias potential = 0.5 V

Mechanism of Enhanced Photocatalytic Activity

On the basis of the above characterization results, the enhanced photocatalytic activity of TC800, compared to that of TC, could be attributed to oxygen vacancies in TiO_2 nanocrystallines and the chemically bonded interfacial contact resulting from the changes in the chemical state of carbon covering, together with the graphite-like carbon. Besides, the different carbon content is also responsible for the difference in photocatalytic activity, since carbon can avoid the direct contact of TiO_2 nanocrystals with dye molecules, which is not conducive to the occurrence of the redox reaction. A possible visible light photocatalytic mechanism of TC800 nanocomposites is proposed in Scheme 1. It is widely accepted that the introduction of oxygen vacancies will result in the visible light absorption[26,36] by bringing intermediate energy levels which are below the lower end of the conduction band at 0.75-1.18 eV.[43] Similarly, the Ti-O-C structure also helps in this regard by introducing some shallow trap states at the surface or intersurface of TiO_2.[44]

Under visible light irradiation, TiO_2 nanoparticles in TC800 are excited and the electrons in the valence band (VB) can easily transfer to the oxygen vacancy level which is below the initial conduction band (CB), resulting in high quantum efficiency and good visible light absorption. Then some of these excited electrons react directly with oxygen adsorbed on the surface of dye molecules and further participate in the redox reactions. Meanwhile, others migrate across the interfaces between TiO_2 nanocrystals and carbon, and are scavenged by graphite-like carbon layer. Then, due to the good conductivity of the graphite-like carbon and the shortened distance caused by the small crystal size of TiO_2, these electrons travel to the surface of the catalyst and are involved in the photocatalytic reaction. At the same time, photo-induced holes in VB quickly react with hydroxyl ions or H_2O to produce hydroxyl radicals which will further oxidize dye molecules. Consequently, electrons and holes are effectively separated, leading to enhanced photocatalytic performance.

In addition, the large specific surface area of TC800 is also beneficial to facilitating the diffusion and adsorption of reactant molecules,[45,46] enhancing light-harvesting and offering vast contact area between the active sites and the reactants.[47,48] Thus, most of the photo-generated holes on the surface react with the adsorbed oxygen and RhB molecules. As with the decomposition of dyes, the adsorption equilibrium is broken and more RhB move from solution to the interface and subsequently are decomposed. Thus, with the combined effect of graphite-like carbon, chemical binding and oxygen vacancies in TiO_2, TC800 shows better photocatalytic performance than TC and even the previously reported TiO_2/non-graphene carbon compounds.

Conclusions

In conclusion, titania/graphite-like carbon nanocomposites with enhanced photocatalytic activity were synthesized via a facile solvothermal approach at 190 °C for 4 h followed by annealing at 800 °C. Further characterization results indicate that the TiO_2 nanocrystals are chemically bonded with the partly graphitized carbon via Ti-O-C. More importantly, oxygen vacancies are successfully introduced into TiO_2 nanocrystals.

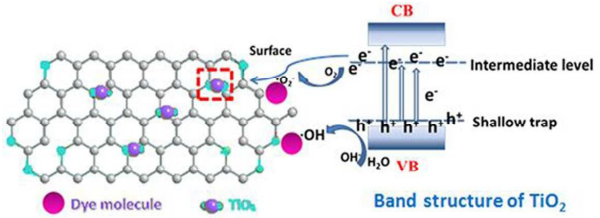

Scheme 1 Schematic illustrations for the synergistic effects of the prepared TiO_2/carbon nanocomposites.

The as-prepared nanocomposites exhibit an enhancement of degradation efficiency that is almost 4 times higher than that of the previously reported TiO_2/non-graphene carbon materials when taking the mass of the dye and catalyst used into account, which is proposed to be a result of the combined effects of oxygen vacancies in TiO_2, chemical binding between TiO_2 and carbon, together with good electric conductivity of the graphite-like carbon.

Acknowledgements

We gratefully acknowledge financial supports from the National Natural Science Foundation of China (Grant No. 51572189, 51372169).

Notes and references

1. J. Du, X. Lai, N Yang, J. Zhai, D. Kisailus, F. Su, D. Wang and L. Jiang, ACS Nano 2011, 5, 590.
2. M. Inagaki, F. Kojin, B. Tryba, and M. Toyoda, Carbon 2005, 43, 1652.
3. K. Hashimoto, H. Irie and A. Fujishima, Jap. J. Appl. Phys., 2005, 44, 8269.
4. N. Li, G. Liu, C. Zhen, F. Li, L. Zhang and H. M. Cheng, Adv. Funct. Mater., 2011, 21, 1717-1722.
5. N. J. Bell, Y. H. Ng, A. Du, H. Coster, S. C. Smith and R. Amal, J. Phys. Chem. C, 2011, 115, 6004-6009.
6. L. W. Zhang, H. B. Fu and Y. F. Zhu, Adv. Funct. Mater., 2008, 18, 2180–2189.
7. X. Wu, M. Sprinkle, X. Li, F. Ming, C. Berger and W.A. Heer, Phys. Rev. Lett., 2008, 101, 026801.
8. S. Gilje, S. Han, M. Wang, K. L. Wang and R.B. Kaner, Nano Lett., 2007, 7, 3394–3398.
9. G. Hu, X. Meng, X. Feng, Y. Ding, S. Zhang and M. Yang, J. Mater. Sci., 2007, 42, 7162-7170.
10. Q. W. Huang, S. Q. Tian, D.W. Zeng, X. X. Wang, W. L. Song, Y. Y. Li, W. Xiao and C. S. Xie, ACS Catal., 2013, 3, 1477−1485.
11. K. Gong, F. Du, Z. Xia, M. Durstock and L. M. Dai, Science, 2009, 323, 760–764.
12. J. Nowotny, T. Bak, M. K. Nowotny and L. R. Sheppard, Int. J. Hydrogen Energy, 2007, 32, 2630.
13. M. K. Nowotny, L. R. Sheppard, T. Bak and J. Nowotny, J. Phys. Chem. C, 2008, 112, 5275.
14. X. Pan and Y.-J. Xu, Appl. Catal. A, 2013, 459, 34-40.
15. F. M. Hossain, G. Murch, L. Sheppard and J. Nowotny, Solid State Ionics, 2007, 178, 319-325.
16. S. N, L. D and K. R, J. Phys. Chem., 1995, 99, 16655–61.
17. X. Chen, L. Liu, P. Y. Yu and S. S. Mao, Science, 2011, 331, 746-750
18. P. J. Feibelman and M. L. Knotek, Phys. Rev. B: Condens. Matter Mater. Phys., 1978, 18, 6531.

19. L. Liu, C. Zhao and Y. Li, J. Phys. Chem. C, 2012, 116, 7904-7912.
20. T. Thompson and J. Yates, Jr, Top. Catal., 2005, 35, 197-210.
21. M. K. Nowotny, L. R. Sheppard, T. Bak and J. Nowotny, J. Phys. Chem. C, 2008, 112, 5275-5300.
22. G. Liu, F. He, X. Li, S. Wang, L. Li, G. Zuo, Y. Huang and Y. Wan, J. Mater. Chem., 2011, 21, 10637–10640
23. H. Ming, H. C. Zhang, Z. Ma, H. Huang, S. Y. Lian, Y. Wei, Y. Liu and Z. Kang, Appl. Surf. Sci., 2012, 258, 3846–3853
24. W. J. Ren, Z. H. Ai, F. L. Jia, L. Z. Zhang, X. X. Fan and Z. G. Zou, Appl. Catal. B, 2007, 69, 138–144
25. S. Shanmugam and A. Gabashvili, Chem. Mater. 2006, 18, 2275-2282.
26. T. Tsumura, N. Kojitani, I. Izumu, N. Iwashita, M. Toyoda and M. Inagaki, J. Mater. Chem., 2002, 12, 1391-1396.
27. N. Q. Zhao, S. Wu, C. N. He, Z. Y. Wang, C. S. Shi, E. Z. Liu and J. J. Li, Carbon, 2013, 57, 130–138.
28. J. C. Parker and R. W. Siegel, Appl. Phys. Lett., 1990, 57, 943–945.
29. C. D. Valentin and G. Pacchioni, J. Phys. Chem. C, 2009, 113, 20543–20552.
30. M. Ramm, M. Ata, K. W. Brzezinka, T. Gross and W. Unger, Thin Solid Films 1999, 354, 106-110.
31. D. Y. Zhang, H. M. Luo, Y. Wang and H. X. Feng, Chem. Lett. 2010, 39, 424-425.
32. J. Sun, H. Zhang, L.-H. Guo and L. Zhao, ACS Appl. Mater. Interfaces, 2013, 5, 13035-13041.
33. L. C. Chen, Y. C. Ho, W. S. Guo, C. M. Huang and T. C. Pan, Electrochim. Acta, 2009, 54, 3884-3891.
34. X. X. Wang, S. Meng, X. L. Zhang, H. T. Wang, W. Zhong and Q. G. Du, Chem. Phys. Lett., 2007, 444, 292-296.
35. Y. L. Lin, T. J. Wang and Y. Jin, Powder Technol., 2002, 123, 194–198.
36. J. Zhong, F. Chen and J. L. Zhang, J. Phys. Chem. C, 2010, 114, 933–939.
37. J. P. Holgado, G. Munuera, J. P. Espino´s and A. R. Gonza´lez-Elipe, Appl. Surf. Sci., 2000, 158, 164–171.
38. P. M. Kumar, S. Badrinarayanan and M. Sastry, Thin Solid Films, 2000, 358, 122–130.
39. D. H. Wang, L. Jia, X. L. Wu, L.Q. Lu and A. W. Xu, Nanoscale, 2012, 4, 576-584.
40. J. S. Lee, K. H. You and C. B. Park, Adv. Mater., 2012, 24, 1084–1088.
41. H. Liu, T. Lv and Z. f. Zhu, J. Molcata., 2015, 404-405, 178-185.
42. M. Y. Xing, J. L. Zhang, F. Chen and B. Z. Tian, Chem. Commun., 2011, 47, 4947–4949.
43. I. Nakamura, N. Negishi, S. Kutsuna, T. Ihara, S. Sugihara and K. Takeuchi, J. Mol. Catal. Chem., 2000, 161, 205-212
44. E. Elmalem, A. E. Sauders, R. Costi, A. Salant and U. Banin, Adv. Mater., 2008, 20, 4312-4317.
45. Z. Liu, D. D. Sun, P. Guo, and J. O. Leckie, Chem. Eur. J., 2007, 13, 1851–1855.
46. X. Wang, J. C. Yu, C. Ho, Y. Hou and X. Fu, Langmuir, 2005, 21, 2552–2559.
47. H. Li, Z. Bian and J. Zhu, J. Am. Chem. Soc., 2007, 129, 8406-8607.
48. Z. Bian, J. Zhu, S. Wang, Y. Cao, X. Qian, and H. Li, J. Phys. Chem. C, 2008, 112, 6258–6262.